Stator-clocking effects on the unsteady interaction of secondary flows in a 1.5-stage unshrouded turbine

T Behr[1*], **A I Kalfas**[2], and **R S Abhari**[1]
[1]Turbomachinery Laboratory, ETH Zurich, Switzerland
[2]Department of Mechanical Engineering, Aristotle University of Thessaloniki, Greece

Accepted paper received by Publisher on 20 April 2007.

DOI: 10.1243/09576509JPE458

Abstract: Effects of stator clocking on the unsteady interaction of stator and rotor secondary flows and performance are investigated in a 1.5-stage, high-pressure turbine. Due to the low aspect ratio design of the blade rows, vortical structures dominate the inlet flow field of the second stator row. Therefore the interaction of first stator and rotor secondary flows in relation to the stator-clocking position must be considered in order to achieve an optimized multi-stage performance.

Four different stator-clocking positions are studied in this experimental investigation. The data comprise unsteady and steady probe measurements, which are acquired downstream of the rotor and the second stator blade row of a 1.5-stage, unshrouded turbine. A two-sensor fast response aerodynamic probe technique is used in the measurement campaign.

It is found that multi-row interaction effects of vortical secondary flow features dominate the loss creation in turbine stages having low aspect ratio geometries. The periodic interaction of shed passage vortices of the first stator with secondary flow structures of the rotor creates regions characterized by reduced total pressure and increased turbulence, and entropy at fixed locations relative to the subsequent stator. Circumferential position of these interaction regions defines the spanwise distribution of total pressure loss in the downstream stator. Stator-clocking controls the spanwise distribution of loss in high-pressure turbines. However, the potential of reducing the loss is limited due to the three-dimensional nature of the flow, and hence, the non-uniform effect of a clocking position on the spanwise performance of a downstream stator.

Keywords: stator clocking, vortex interaction, high-pressure turbine, multi-stage effects

1 INTRODUCTION

The quest for improved turbine efficiencies to reduce fuel consumption and weight drives designers to gain a better understanding of unsteady blade row interactions. Clocking of stator rows has the potential to control the interaction mechanisms of secondary flows of subsequent blade rows that create losses. Since the ratio of flow field areas affected by wakes and vortices depends on the aspect ratio of a turbine, designers have to account for these different mechanisms to find an optimum clocking position. For example vortical flow structure can influence up to 50 per cent of the span in high-pressure turbine geometries.

The effect of clocking on turbine efficiency has been demonstrated in a number of studies (experimental: Huber *et al.* [**1**], Gombert and Höhn [**2**], Reinmöller *et al.* [**3**], Tiedemann and Kost [**4**]; numerical: Bohn *et al.* [**5**]). In these studies the circumferential position of the wake of the upstream stator relative to the leading edge of the subsequent stator was mainly held responsible for the effect on efficiency. Contrary effects of clocking positions on different span regions have been found by Behr *et al.* [**6**], Huber *et al.* [**1**], Schennach *et al.* [**7**], and Arnone *et al.* [**8**]. Consequently, they all suggested to focus more on the three-dimensionality of the flow for explaining clocking phenomena. This aspect is especially important in high pressure, low aspect ratio turbines geometries

Corresponding author: Turbomachinery Laboratory, ETH Zurich, Switzerland. email: thomas.behr@gmx.net

(Haldeman *et al.* [**9**], Schennach *et al.* [**7**], Gadea *et al.* [**10**], Hummel [**11**]). In this context, vortex transport in low aspect ratio turbines becomes important (Miller *et al.* [**12**], Gaetani *et al.* [**13**], Chaluvadi *et al.* [**14**]).

In order to numerically simulate the interaction between different vortex systems, unsteady multi-row calculations are required. Due to the complex nature of these flow phenomena and the limited experimental data background, there are very few approaches that are able to simulate this kind of interactions.

In this study, flow field data have been measured in a low-aspect ratio, high-work, 1.5-stage turbine with a high spatial and temporal resolution at different clocking positions. Based on this database, the effect of vortex and blade row interaction on the performance of a subsequent stator is investigated.

2 EXPERIMENTAL METHOD

2.1 Research turbine

The air-loop of the facility is of a quasi-closed type and includes a radial compressor, a two-stage water-to-air heat exchanger and a calibrated venturi nozzle for mass flow measurements. Before the flow enters the turbine section, it passes through a 3-m long straight duct, which contains flow straighteners to ensure an evenly distributed inlet flow field. Downstream of the turbine the air-loop is open to atmospheric conditions. A DC generator absorbs the turbine power and controls the rotational speed of the turbine. A torque meter measures the torque that is transmitted by the rotor shaft to the generator. The turbine entry temperature is controlled to an accuracy of 0.3 per cent and the r/min is kept constant within $\pm 0.5\,\mathrm{min}^{-1}$ by the DC generator. The pressure drop across the turbine is stable within 0.3 per cent for a typical measurement day. More information on the test rig can be found in articles by Behr *et al.* [**15**] and Sell *et al.* [**16**]. A cross-section cut and the key parameters of the turbine configuration are presented in Fig. 1.

2.2 Measurement technology

Experimental flow field data presented in the paper are derived from time-resolved and pneumatic probe measurements in planes downstream of each blade row. Pneumatically averaged flow field has been measured using a 0.9-mm diameter

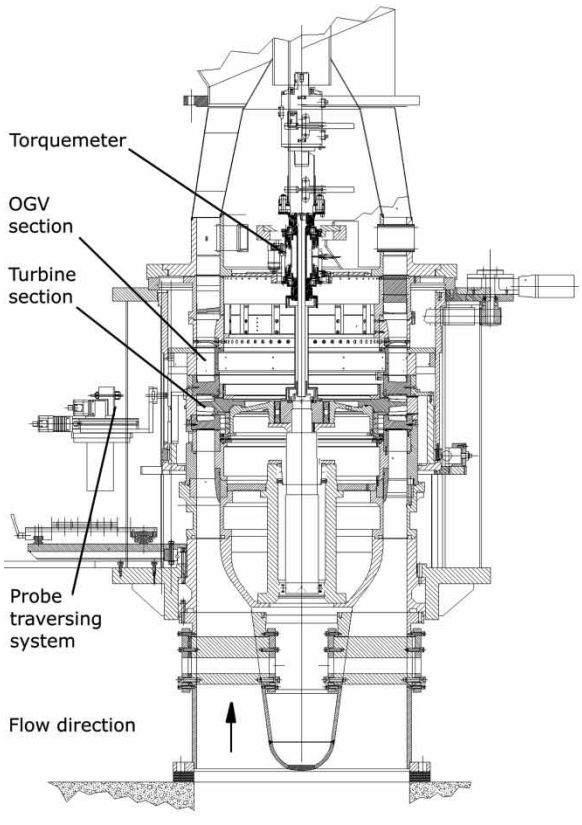

Turbine	
Rotor speed [RPM]	2700
Pressure ratio (1.5-Stage, total-to-static)	1.60
Turbine entry temperature [°C]	55
Total inlet pressure [bar abs norm]	1.4
Mass flow [kg/s]	12.13
Shaft Power [kW]	292
Hub/Tip diameter [mm]	660/800

1st Stage	
Pressure ratio (1st Stage, total-to-total)	1.35
Degree of reaction [-]	0.39
Loading coefficient $\psi=\Delta h/u^2$ [-]	2.36
Flow coefficient $\phi=c_x/u$ [-]	0.65

Bladerows		
Number of blades	Stator 1	36
	Rotor	54
	Stator 2	36
Reynolds number based on true chord and blade row relative exit velocity [-]	Stator 1	$7.1\cdot10^5$
	Rotor	$3.8\cdot10^5$
	Stator 2	$5.1\cdot10^5$
Blade row relative exit Mach numbers [-] (average)	Stator 1	0.54
	Rotor	0.50
	Stator 2	0.48

Fig. 1 LISA one-and-1/2-stages axial turbine facility

cobra-head five-hole probe (Behr *et al.* [**17**]). The unsteady pressure measurement technology of the fast response aerodynamic probes (FRAP) has been developed at the Turbomachinery Laboratory (Kupferschmied *et al.* [**18**], Pfau *et al.* [**19**]). The flow fields were measured using a novel 1.8 mm tip diameter, two-sensor FRAP probe in virtual-four-sensor mode to provide two-dimensional, time-resolved flow field information. Each measurement plane is resolved on a grid of 39 points in the radial direction that are clustered close to the endwalls and 20 equally spaced points in the circumferential direction, covering a stator pitch. The time-resolved pressure signals are acquired at each measurement point at a sampling rate of 200 kHz over a time of 2 s. Data sets are processed to derive basic flow quantities, i.e. total and static pressure, flow yaw and pitch angles, velocity components and Mach number by phase lock averaging over 85 rotor revolutions. For the data analysis, three consecutive rotor passages were selected. Each rotor passage is resolved in time by 82 samples. The frequency response of the probe captures flow features at frequencies up to 35 kHz. With the two-sensor probe technology it is possible to obtain also flow turbulence information (Porreca *et al.* [**20**]). For this purpose the non-deterministic variation of the probe signal over 85 rotor revolutions is examined. The FRAP probe technology provides also temperature data at frequencies up to 10 Hz.

2.3 Test cases and data presentation

For the present investigation four stator–stator relative positions have been examined with a circumferential spacing of 25 per cent of a stator pitch. The time-resolved flow field is measured for all clocking positions at the rotor exit and for the 0 per cent clocking position at both stator exits. In addition all clocking positions are measured at rotor and stator 2 exits with a pneumatic five-hole probe. Figure 2 shows an exact depiction of relative profile positions. Since the investigation of unsteady blade row interactions requires a reliable knowledge of the relative position of stators and rotor, the time-resolved rotor position is shown as well in Fig. 2. The rotor blade-passing time scale t/T and the stator pitch scale are consistent with the scales in the subsequent plots presented in this paper. In this way it is possible to correlate flow phenomena with their associated relative profile positions. All contour plots of the flow fields presented are views in downstream direction. The rotor turning direction in the plots is accordingly from the left to right.

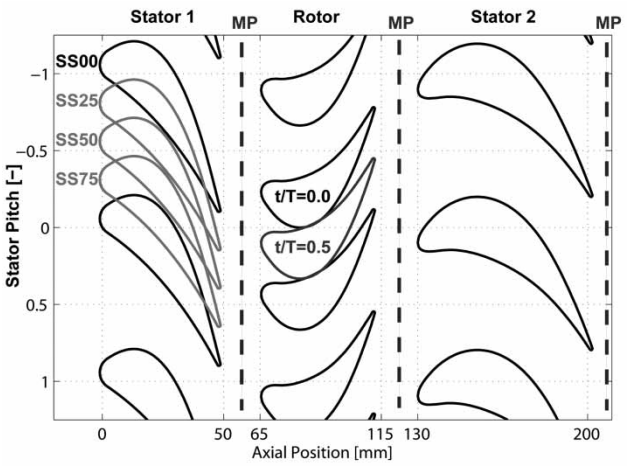

Fig. 2 True length visualization of the investigated turbine profiles at midspan, including stator-clocking positions, stator–rotor relative positions and positions of measurement planes

3 RESULTS AND DISCUSSION

The exit flow fields of both first and second stator are measured with a five-hole pneumatic probe. Figure 3 shows the distribution of total pressure coefficient at both stator exits. A detailed analysis of the steady and unsteady flow fields of the turbine under consideration can be found in the article by Behr *et al.* [**15**]

$$Cpt = \frac{p_t - p_{s,\text{TurbineExit}}}{p_{t,\text{TurbineInlet}} - p_{s,\text{TurbineExit}}}$$

According to the classical secondary flow theory, in both flow fields the positions of the passage vortices and the wake can be anticipated based on the regions of reduced total pressure. In the stator 1 exit flow, the passage vortices are located relatively close to the endwalls at 10 and 80 per cent span. Due to the swirling flow, the vortex tubes are cut by the measurement plane at an oblique angle and appear as ellipses in the contour plot. In between the two vortices the wake of the stator profile is aligned in the radial direction with a circumferential extension of about 20 per cent of a stator pitch. The flow between the two stator wakes experiences almost no reduction in total pressure, which results in larger area of homogeneous flow with a rather constant total pressure. In contrast to this, the exit flow field of the second stator reveals a large region with considerably reduced total pressure in addition to the reduced total pressure at the vortex and wake positions (Fig. 3(b)). Only a region between 30 and 60 per cent span, extending from the pressure side boundary of the stator wake until midpitch, can be considered to be almost unaffected by total pressure loss due to secondary flows. The additional reduction of total pressure within the second stator compared to the first one has to be attributed to the effects of the rotor exit flow, which disturbs the stator inlet flow field. Since this turbine case has a low aspect ratio

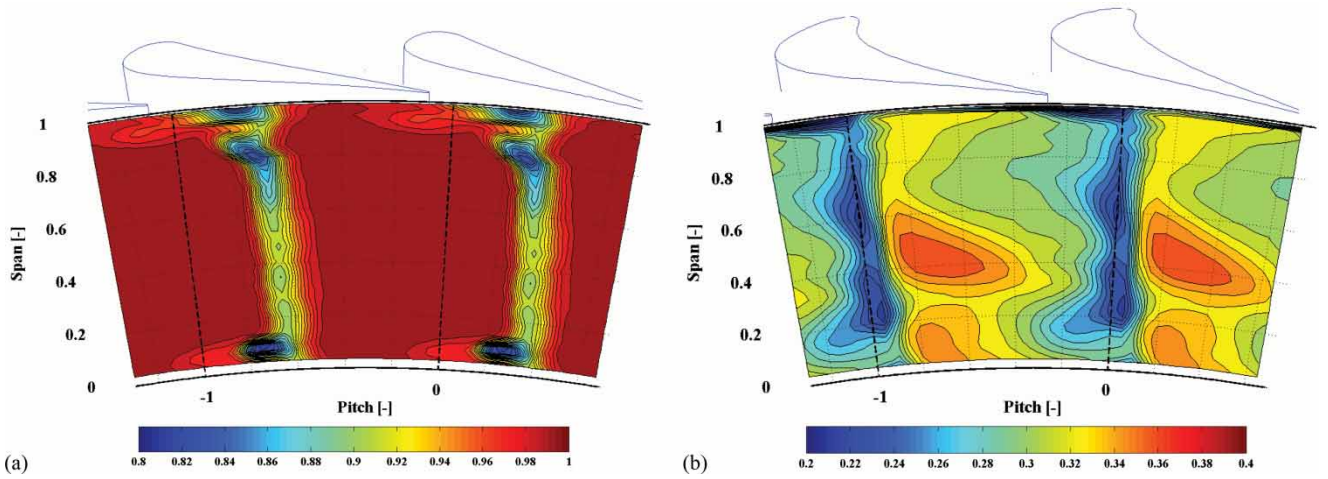

Fig. 3 Total pressure coefficient *C*pt at: (a) stator 1 exit (b) stator 2 exit

blading, the rotor vortices are thought to contribute most to this disturbance. Hence, the inlet flow field of a stator embedded in a multi-stage turbine environment seems to play a critical role on the performance of this blade row.

According to these findings, the following discussion tries to increase the understanding of the flow effects that influence the second stator inlet flow and the impact that they have on performance and outlet flow field of the second stator. By clocking the first stator row relative to the second one, the effects of stator 1–rotor interaction and rotor–stator 2 interactions can be evaluated separately.

The discussion starts with the evaluation of the time-resolved secondary flows originating in the rotor. The influence of stator clocking on the rotor secondary flows is discussed in the following section, since they are significantly affected by the secondary flows of the first stator. Afterwards the flow field and the performance of the second stator are evaluated.

3.1 Unsteady rotor secondary flow

The overall effects on the performance of a stator row can be judged most effectively from time-averaged flow field visualizations in the stationary frame of reference. In such plots, flow parameters of a rotating blade row that is not affected by a stator show only gradients in radial direction. Variations in circumferential direction can be only due to influences of stationary blade rows. In order to understand better the time-averaged contour plots in the next section, the time-resolved rotor exit flow field is discussed first.

Since secondary flow features are inherently associated with an increased level of flow unsteadiness, it is possible to trace and evaluate the features from their turbulence intensity. Figure 4 shows the distribution of turbulence intensity of the 0 per cent clocking case at four equidistant time steps within one rotor blade-passing period. The traces of three rotor vortices can be observed at 20 per cent span (hub passage vortex), 75 per cent (tip passage vortex) and 95 per cent span (tip leakage vortex). The leading edges of the second stator are approximately located at stator pitch positions −1 and 0. In Fig. 4 the tip passage vortex is circled by a dotted line for all four time steps. It can be seen that as this vortex region passes the stator leading edge, the turbulence intensity reduces by factor 2. The same effect has been described in more detail in the article by Behr *et al.* [**6**]. Depending on the relative

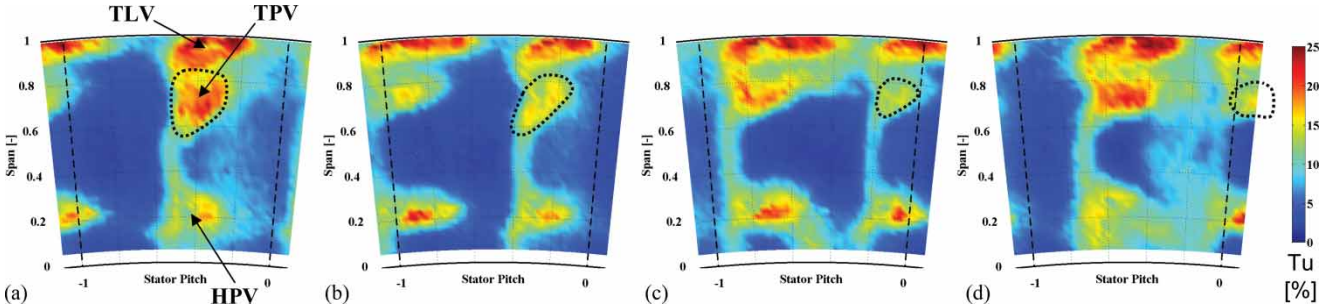

Fig. 4 Turbulence intensity (per cent) at rotor exit (SS00) at four equidistant time steps within one rotor blade-passing period: (a) $t/T = 0$, (b) $t/T = 0.25$, (c) $t/T = 0.5$, (d) $t/T = 0.75$

positions of the rotor and second stator, the vortex is modulated by the stator profiles and shows a variation in size and relative position to the rotor trailing edge when it stretches around the stator leading edge. Also the tip leakage vortex and the hub passage vortex show a similar behaviour. However, the reduction in turbulence intensity appears to be less when they pass the second stator leading edge. Since these two vortices have the same sense of rotation, in contrast to the tip passage vortex, it is assumed that the periodic reduction of turbulence depends on the sense of rotation of a vortex.

3.2 Interaction of stator 1 and rotor secondary flows

The flow field of the first stator including its secondary flow features convects into the subsequent rotor. The rotor divides the stator flow into periodic portions, which get transported through a rotor passage. Depending on the nature of the incoming flow features, they are affected differently by the rotor. Vortices get bent and stretched around the rotor leading edge. Wakes get chopped by the rotor. As wakes and vortices pass through the rotor, the stator secondary flow features interact with the developing rotor secondary flows. The rotor secondary flow is produced continuously by the rotor, in contrast to the stator secondary flows, which appear periodically inside the passage. Hence, the outlet flow of the rotor has also a periodic character in the rotor relative frame. The products of these periodic interactions of stator 1 and rotor secondary flows are transported by the rotor to fixed locations in the stationary frame at the inlet of the second stator. Therefore, it is reasonable to evaluate time-averaged flow contours at the inlet to the second stator, in order to understand the influence of the upstream stator. For a better understanding of the flow mechanisms involved, an analysis of the time-resolved flow is still indispensable.

3.2.1 Time-averaged flow field

Figure 5 shows a matrix of time-averaged contour plots of the rotor exit flow field in terms of the total pressure coefficient, turbulence intensity and entropy in the horizontal direction, and four clocking positions in the vertical direction. The total pressure coefficient is obtained from pneumatic five-hole probe measurements. The turbulence intensity is derived from the time-resolved FRAP two-sensor probe measurements. The entropy difference is calculated following Denton [**21**] using the total pressure distribution of the five-hole probe and the total temperature information obtained from the FRAP 2-sensor measurement. As a reference point for the entropy calculation the turbine inlet conditions are used. It should be emphasized again that all variations in circumferential direction are caused by either the upstream or the downstream stator. For the current investigation the upstream stator is moved to achieve a stator-clocking effect. The coordinate system of the probe as well as the position of the second stator remains unchanged through all clocking cases according to Fig. 2.

In Fig. 5, three flow regions are highlighted, which move together with the stator clocking position in circumferential direction. This fact implies that the origin of these flow regions is the first stator.

3.2.1.1 Region A (Tip). This flow region marks the interaction between the remnants of the first stator tip passage vortex and the rotor tip leakage and tip passage vortex. It is characterized by an increased level of turbulence intensity with maxima at the span positions of the rotor tip passage vortex and the tip leakage vortex. The same region the time-averaged total entropy shows increased values, which correspond qualitatively with the turbulence intensity. In this case a clear connection between high turbulent flow and increased losses due to viscous dissipation is seen. Interestingly, in the time-averaged contour plots there is no clear evidence of a reduction of absolute total pressure related to this flow region. However, in the time-resolved contours (Fig. 6) a periodically appearing region of low total pressure is detected (S2). It is later discussed more in detail.

The flow mechanism, which causes this periodic increase of turbulence in this region, is the result of the interaction of several vortices located in the tip region. The tip leakage vortex is continuously produced by the rotor and is located in the corner between tip endwall and rotor suction side. The vortex appears in the rotor passage at the approximate position of the suction side peak, which is at around 50 per cent rotor axial chord. Next to the tip leakage vortex, the passage vortex of the rotor develops out of the cross-passage flow at the tip endwall. It is counter rotating to the tip leakage vortex and is placed more radially inwards at around 80 per cent span at the rotor suction side. This system of two counter rotating vortices gets under the periodic influence of the tip passage vortex of the upstream stator. The vortex tube of the stator tip passage vortex leaves the stator at the radial position of around 80 per cent span with a yaw angle of around 73°. As this vortex bends around the rotor leading edge it creates a counter rotating pair of horseshoe vortices, which get transported through the rotor passage. The pressure side leg of this vortex is drawn across the passage towards the suction side of the adjoining rotor blade. During this process it merges with the rotor passage vortex, which has the same sense of rotation. This periodic interaction results in a periodically strengthened rotor tip passage vortex. The suction side leg of

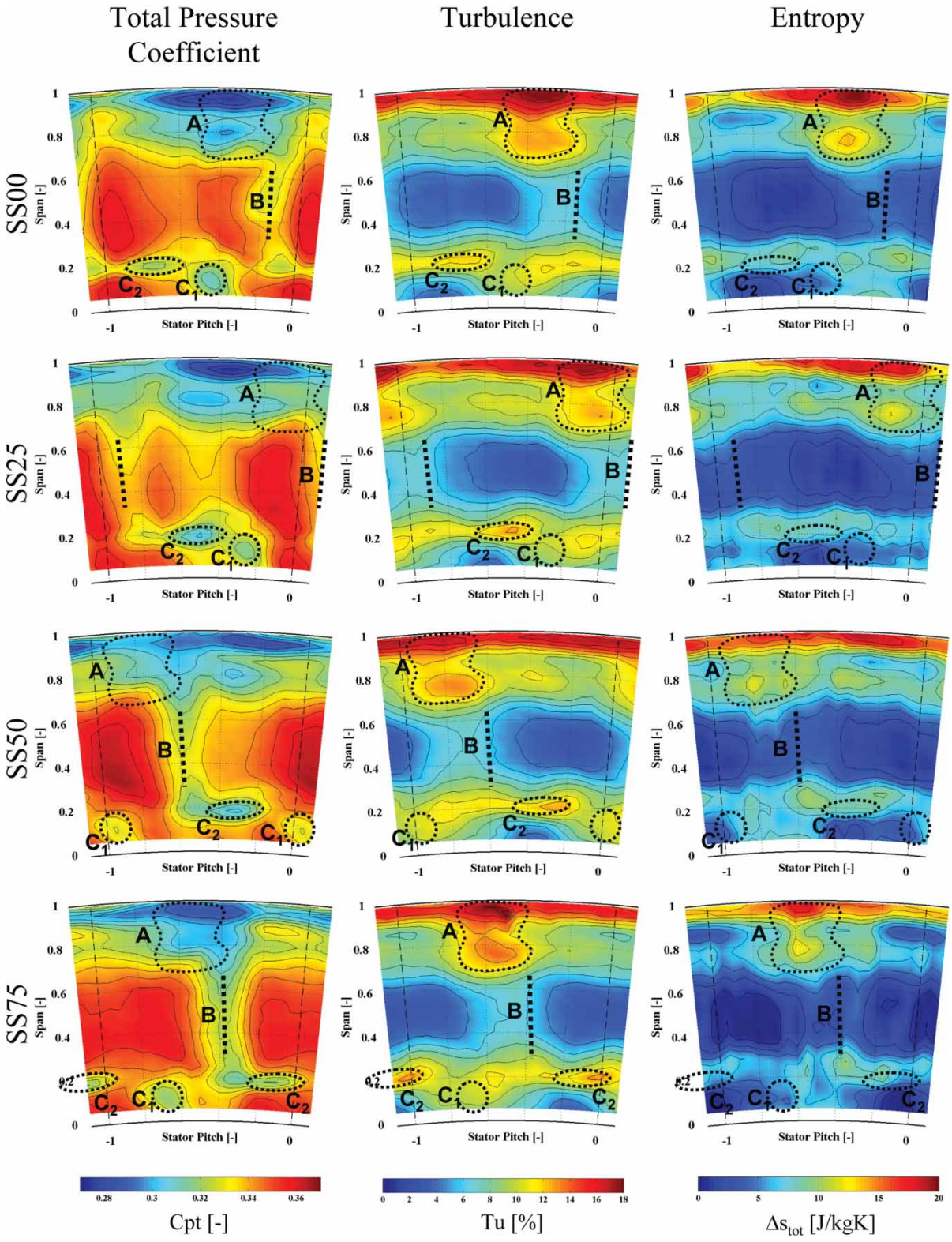

Fig. 5 Time-averaged rotor exit flow field for four stator-clocking positions: total pressure coefficient *C*pt, turbulence, and total entropy difference

the stator passage vortex stays attached to the suction side of the rotor blade. This vortex has the same sense of rotation as the rotor tip passage vortex, which is located at the same radial position in the passage. The proximity of the two vortices with the same sense of rotation leads to the production of increased losses

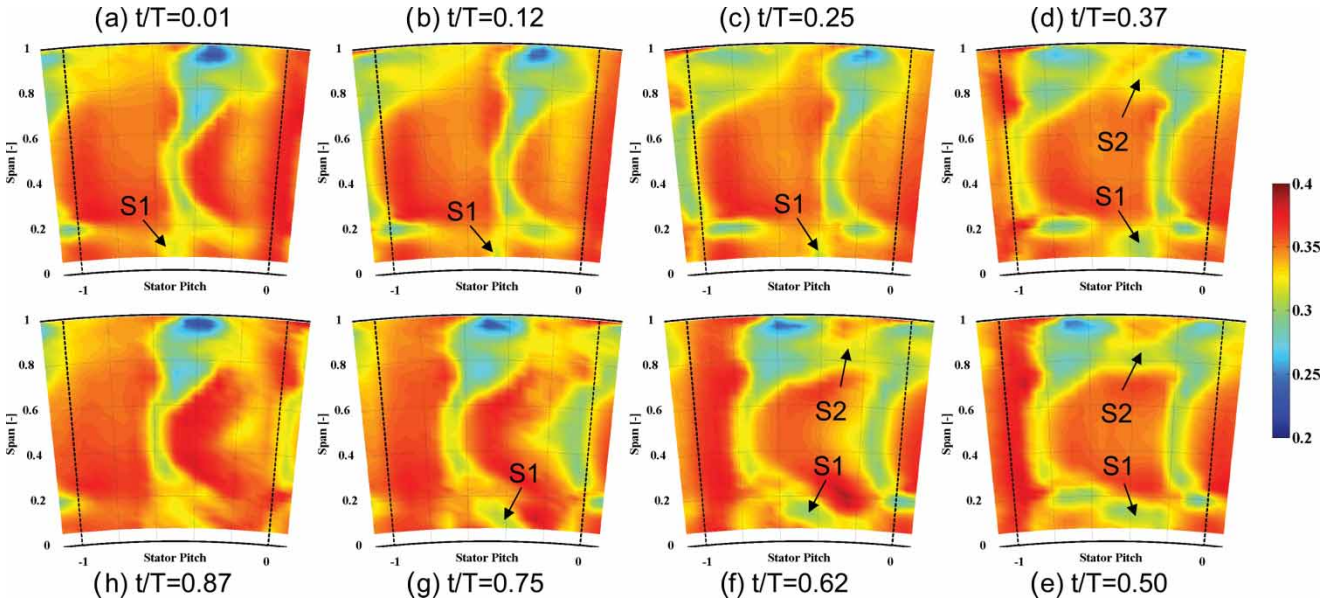

Fig. 6 Time-resolved contours of absolute total pressure coefficient at rotor exit at SS00

due to viscous shear. This loss production can be seen in the increased level of entropy in region A. Further it causes an increase in turbulence intensity. Due to the periodic occurrence of the stator passage vortex in the rotor passage, the interaction region with higher entropy and an increased turbulence level appears consequently at a fixed location in the rotor exit flow field (region A).

It has been mentioned before, that the turbulence intensity drops if a vortex approaches the circumferential position of the second stator leading edge. The same phenomenon can be recognized at the 25 per cent stator clocking position (SS25). In this case the turbulence level of region A is the lowest compared to the other three clocking cases.

3.2.1.2 Region B (Midspan). This flow region represents the approximate position of the flow that originates from the first stator wake. It can be clearly identified by the deficit in absolute total pressure. It is remarkable that the circumferential position of the minimum in total pressure does not coincide exactly with the maximum of the turbulence intensity. Between the two, a circumferential offset of about 10 per cent of stator pitch can be found.

3.2.1.3 Region C (Hub). In the hub region two flow features that move together with the stator-clocking position are detected, marked as C1 and C2 in Fig. 5. It has to be kept in mind that the rotor hub passage vortex passes at 20 per cent of the rotor span. Region C1 is confined between the trace of the rotor hub passage vortex and the hub endwall. It clearly shows a reduced level of absolute total pressure, which coincides with an increased level of turbulence. Close to C1 another region appears that moves together with the stator-clocking position. This region, named C2, is also characterized by a higher level of turbulence and lower total pressure.

The flow mechanisms that are responsible for the local increase of turbulence at C1 and C2 are explained in the following. As the vortex tube of the stator hub passage vortex interacts with the leading edge of the rotor, it bends around the profile and creates a pair of horseshoe vortices (see Fig. 7). The pressure side leg of the stator passage vortex has the same sense of rotation as the rotor indigenous passage vortex. Since at the exit of the rotor only one vortex appears with this rotation, the rotor passage vortex must have merged with the pressure side leg of the stator vortex. The suction side leg of the stator hub passage vortex convects through the rotor passage in the corner of the suction side and the hub endwall. Due to its sense of rotation it stays attached to the hub endwall. Therefore, this suction side leg of the stator hub passage vortex appears

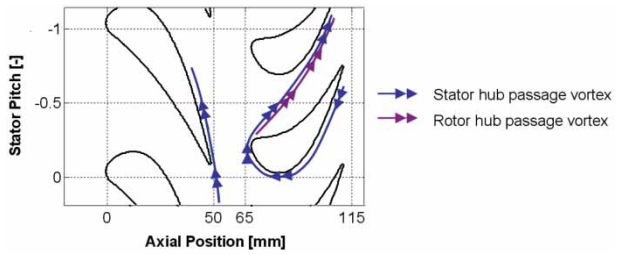

Fig. 7 Vorticity vectors at the hub endwall of stator 1 and rotor

attached to the endwall at the region C1 at the exit of the rotor passage.

Inside the rotor passage the counter rotating vortex tubes of the rotor hub passage vortex and the suction side leg of the stator hub passage vortex interact with each other, since they both get convected in parallel along the suction side. The interaction process results in an increased turbulence level of the rotor hub passage vortex in the rotor outlet plane, which is indicated by the flow region C2.

Since the two legs of the stator hub passage vortex convect periodically through the rotor passage, the interaction that is observed at the rotor exit appears as well periodically. It is, therefore, advantageous to analyse the time-resolved flow field data in order to get better insight into the interaction of the secondary flows.

3.2.2 *Time-resolved flow field*

The previous section has discussed the products of the periodic interaction of remnants of the first stator secondary flow and the rotor secondary flow on the basis of time-averaged contour plots. This subchapter sheds more light on the interaction process by evaluating the time-resolved measurement results. To visualize the flow interaction, Fig. 6 shows the contours of the absolute total pressure coefficient of the SS00 clocking case in eight equidistant time steps of one rotor passing period.

3.2.2.1 Region A (Tip). Remnants of the first stator tip passage vortices can be identified as a low total pressure region, which appears for about 30 per cent of the time of one rotor blade-passing period (see S2 in Figs 6(d) to (f)). As the rotor tip vortices move on with the rotor, this region remains at a constant pitch position relative to the stator. The low total pressure region of the next rotor blade merges later with the flow feature S2.

The marked effect that the flow feature S2 has on the turbulence intensity of the rotor tip secondary flow region is visualized in Fig. 8 for the clocking positions SS25 and SS75. The figure shows the evolution of turbulence intensity at the radial position of the rotor tip passage vortex, for the two oppositional clocking positions. In such time–distance plots flow features, which are fixed to the stators appear in the vertical direction. Flow patterns travelling with the rotor can be seen as diagonal traces in the contours. The positions of rotor trailing edges and stator 2 leading edges are marked with dashed lines in the plots. In the figure it can be seen that the turbulence intensity increases suddenly at the pressure side of the rotor. As the rotor moves on, the high turbulent region of the next rotor blade merges with region S2. In the time–distance plots it can be seen that the S2 region is sharply confined on

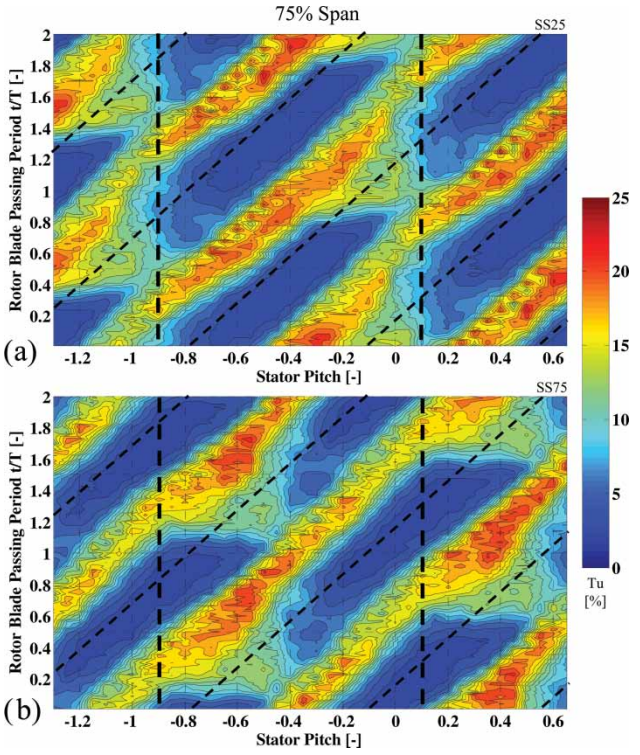

Fig. 8 Turbulence versus blade-passing period at rotor exit (75 per cent span): (a) SS25, (b) SS75

the right side, which means that it does not move in the rotor direction. Further, with these plots of two clocking positions it can be demonstrated that the turbulence level of the vortices decreases if they get under the influence of the potential field of the downstream stator leading edge. Following the inclined trace of the rotor vortices in the contour plots it can be seen that the turbulence level reduces as they approach the stator pitch positions −1 and 0. These positions correspond approximately to the position of the second stator leading edges. One has to keep in mind that the vortices pass through the measurement plane with a swirl angle of around −40°. Hence, in the case that the rotor vortices show a reduced level of turbulence, they do not hit the stator leading edge. This fact has been visualized in Fig. 9. It shows the centre of region A, as it was found in the time-averaged contours of turbulence in Fig. 4, and its average flow direction, derived from the mass-averaged flow yaw angle of region A. One can see that in the case of reduced turbulence in the interaction region A at SS25 the flow passes the second stator leading edge at its suction side.

3.2.2.2 Region C (Hub). In the time-averaged contours the flow region C1 originating from the suction side leg of the stator hub passage vortex has been identified at the hub. In the time-resolved contours of the total pressure coefficient (see Figs 6(a) to (g)) this region appears periodically at a fixed location at

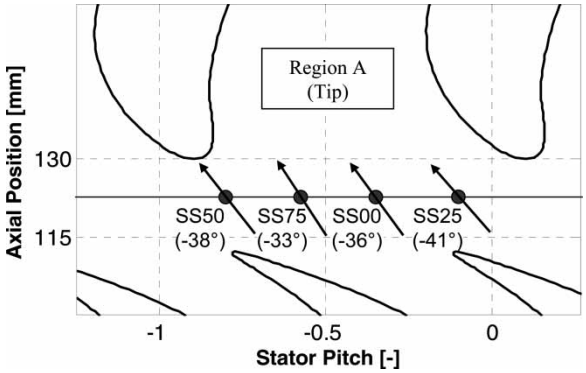

Fig. 9 Circumferential position and flow direction of region A (see Fig. 5) for four clocking positions

the hub. It is marked with the label S1 in the contours. Similar to S2 it appears at the pressure side of the rotor exit flow. In the following time steps the low total pressure region S1 of the suction side leg of the stator passage vortex lifts off from the hub region and seems to move slightly in the opposite direction of the rotor. In the following time steps the pressure contours show the interaction of the rotor hub passage vortex with the stator passage vortex leg. During the time of interaction the rotor passage vortex is displaced radially away from the endwall by the stator passage vortex.

The relative position of the rotor hub passage vortex and the stator hub passage vortex within the rotor passage is visualized in a three-dimensional schematic in Fig. 10. The pressure and suction side leg of the stator passage vortices involved in the vortex interaction originate from two neighbouring stator profiles. This fact is visualized in the figure by different colours of the vortex tubes, each of them representing the secondary flow of upstream stator passage.

This radial order of the two vortices is opposite to the one presented by Chaluvadi *et al.* [**22**]. They traced the path of the stator passage vortex in the rotor with

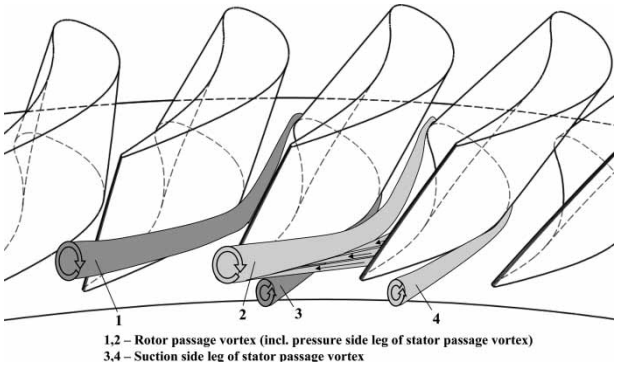

Fig. 10 Three-dimensional schematic view of the relative position of rotor hub passage vortex and stator hub passage vortex within the rotor passage

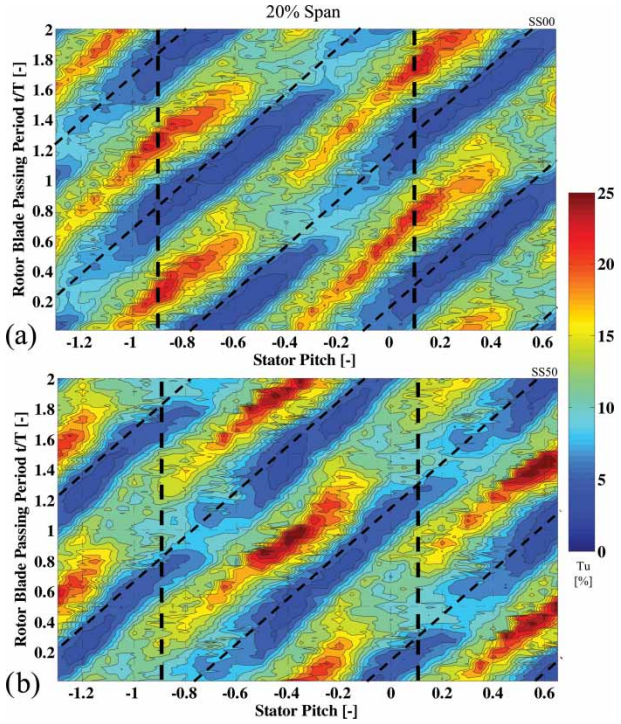

Fig. 11 Turbulence versus blade-passing period at rotor exit (20 per cent span): (a) SS00, (b) SS50

smoke visualization in a low speed turbine rig. It was found that the rotor hub passage vortex stays at the endwall, while the stator vortex is displaced radially into the passage.

The interaction of the rotor hub passage vortex and the remnant of the stator vortex can also be seen in the time–distance diagram of the turbulence intensity at 20 per cent span (Fig. 11). At the time instant of the interaction the turbulence intensity in the region of the rotor hub passage vortex reduces by 50 per cent, and its absolute total pressure deficit diminishes. This interaction can be seen in the contour plot of turbulence intensity, where the diagonal traces of high turbulence are periodically interrupted for about 20 per cent of a rotor blade-passing period. Within this time period of the interaction the level of turbulence in the region of the rotor vortex reduces, whereas the turbulence level in the region of the passage flow increases. This behaviour indicates that the rotor passage vortex gets distorted and deflected due to the influence of the stator hub passage vortex. As a consequence the entire passage flow in this span region is characterized by a higher level of turbulent kinetic energy during the interaction.

3.3 Second stator flow field

It has been shown in the previous section that the inlet flow field of the second stator can be influenced by the stator clocking. Further it has a periodic character,

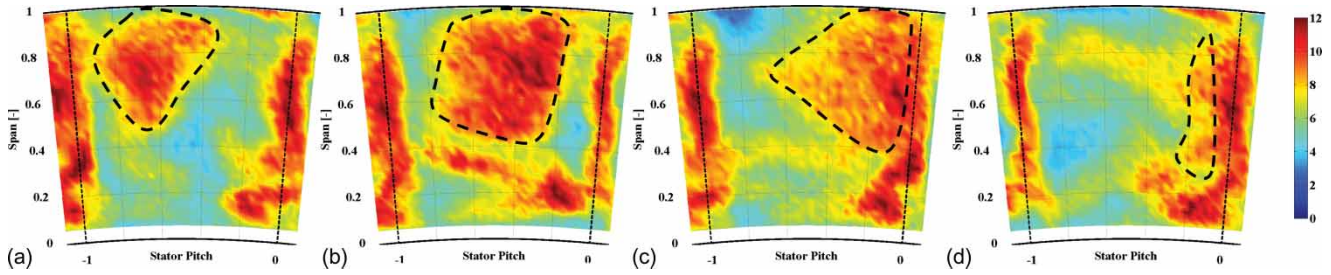

Fig. 12 Turbulence intensity (per cent) at stator 2 exit (SS00) at four equidistant time steps within one rotor blade-passing period: (a) $t/T = 0$, (b) $t/T = 0.25$, (c) $t/T = 0.5$, (d) $t/T = 0.75$

which is introduced by the rotor. Within the second stator secondary flow features are created continuously due to viscous effects on the boundary layers. These influences are superimposed and interact with each other inside the second stator. At the stator exit plane the result of this interaction can be evaluated. Periodicity appearing in this plane can only be assigned to the upstream rotor, since there is no blade row further downstream.

Figure 12 shows contours of the turbulence intensity level of four equidistant time steps within one rotor blade-passing period. At stator pitch position 0 a steady region of increased turbulence associated to the stator wake can be seen extending from 20 to 80 per cent span in radial direction. In addition a periodically appearing region of increased turbulence can be identified between 50 and 100 per cent span; this originates from the upstream rotor. More precisely, it is thought that this region represents the remnants of region A in Fig. 5. It is marked with a dashed line in Fig. 12. It appears close to the pressure side of the stator and moves in the rotor direction until it merges with the high turbulence region of the stator wake. Since it occupies up to 50 per cent of the stator exit flow field it is expected that it has a major influence on the loss creating mechanisms, and hence, on the performance of the stator. Dejc and Trojanovskij [**23**] conclude that generally the losses increase with increasing turbulence levels. It was found that upstream turbulence advances the boundary layer transition on the profile suction side. Figure 13 presents the timewise evolution of this high turbulence region. The diagonal lines mark the position of the rotor trailing edges (see Fig. 2). From this figure it can be seen that the remnants of region A appear 20 per cent of a stator pitch apart from the stator wake on the pressure side of the passage. As it migrates to the suction side a time delay relative to the rotor motion by about 50 per cent can be seen. This fact indicates that flow features from the rotor are transported with a different axial velocity through the stator depending on the pitchwise position within the stator passage.

The behaviour of the unsteady exit flow of the second stator has been discussed briefly. It is now

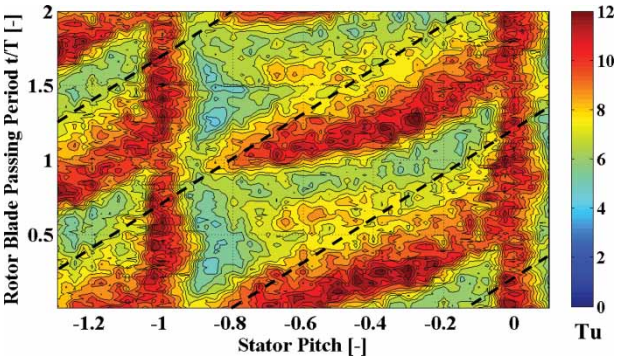

Fig. 13 Turbulence intensity (per cent) at stator 2 exit (SS00, 75 per cent span) versus rotor blade-passing period

important to see how the unsteady flow is represented in time-averaged flow contours of the second stator, which give a more clear representation of the stator performance. For this purpose the time-averaged contours of turbulence intensity are shown in Fig. 14 together with the time-averaged distribution of total pressure coefficients. It can be seen that the time-averaged turbulence intensity in the region of the periodic flow feature is about 40 per cent higher than in the freestream. If one compares the total pressure contours with the turbulence intensity contours, a clear relationship can be seen. Regions of high turbulence correspond to a region of low total pressure. From this observation it can be concluded that the periodic flow feature from the rotor reduces the total pressure in the stator exit plane between 50 and 100 per cent. An analysis of the stator performance is presented in the next section.

In Fig. 15 the influence of the stator clocking on the exit flow field of the second stator is demonstrated. Depending on where a flow feature that leaves the rotor hits the second stator, it causes different reduction in total pressure in the stator passage. The total pressure contours for four different clocking positions are presented in Fig. 15. It has been found that the area affected by region A of the rotor exit flow field extends well into the midpitch region for the 0 and 25 per cent

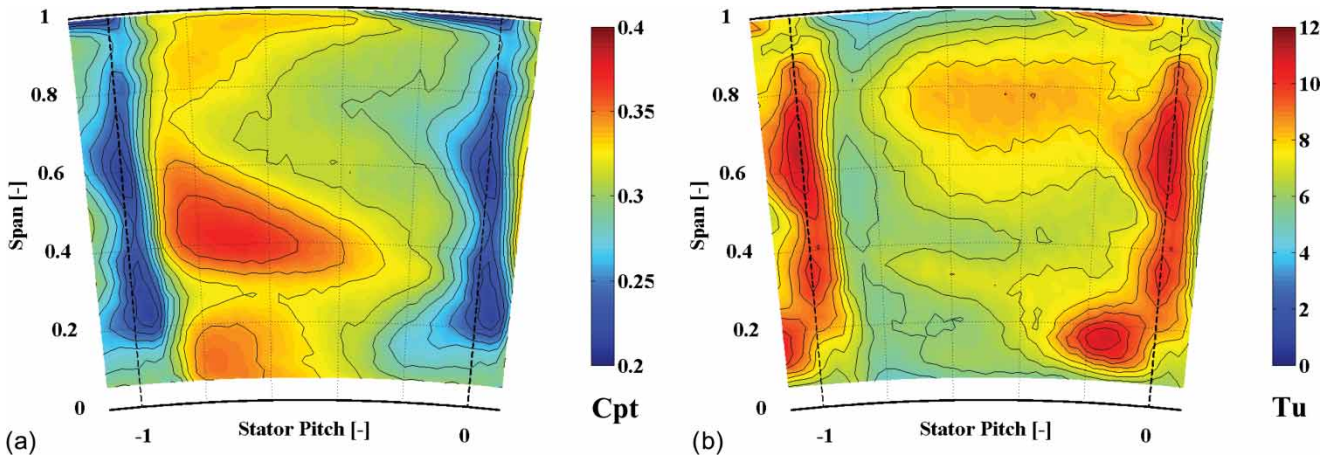

Fig. 14 Time-averaged contours at stator 2 exit (SS00) of: (a) total pressure coefficient(−), (b) turbulence intensity (per cent)

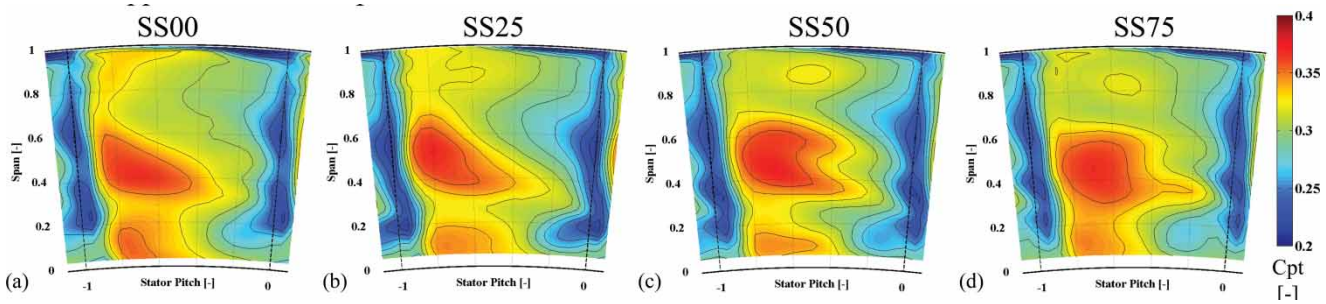

Fig. 15 Total pressure coefficient *C*pt(−) at stator 2 exit at four clocking positions: (a) SS00, (b) SS25, (c) SS50, (d) SS75

clocking cases. In these cases region A passes the second stator leading edge close to its suction side. At the other two positions (50 and 75 per cent stator clocking) the low total pressure region is confined between 60 and 100 per cent span. However it seems to appear closer to the pressure side of the stator wake.

3.4 Second stator performance

The effect of the stator clocking on the exit flow field of the second stator has been discussed in the previous section. In this chapter it is shown how these qualitative observations translate into pitchwise averaged performance values.

Figure 16 shows the pitchwise mass-averaged area-specific massflow distribution across the span at stator inlet and exit for all four clocking positions. As expected, the differences at the stator inlet are negligible, which confirms that the upstream effect of the second stator is weak and that the stator clocking does not change the capacity of the turbine. However, the different secondary flow interaction mechanisms related to the clocking position cause a significant redistribution of massflow within the second stator (see Fig. 16(b)).

Figure 17 shows the spanwise distribution of the total pressure loss coefficient of the second stator (Denton [**21**]). The extended uncertainty ($k = 2$, 95 per cent coverage) of the required total pressure and static pressure is ±80 and ±95 Pa, respectively (Behr *et al.* [**17**]). Thus, the extended uncertainty of the total pressure loss coefficient amounts to ±0.01. In order to take into account the redistribution of massflow, the calculation of the coefficient takes into account the change of streamtube thickness across the stator. The fact that loss coefficient values within 10 per cent span away from the casing are less than zero, is probably due to the fact that a pneumatic five-hole probe encounters problems in a highly unsteady flow, such as within a tip leakage vortex of a rotor. Figure 17 shows that total pressure loss across a rotor changes with the stator-clocking position. In order to quantify this effect further, Fig. 18 summarizes the total pressure loss coefficients of different span regions. Hereby the 'Tip' region can be associated to region A, 'Midspan' to region B and 'Hub' to regions C1 and C2 shown in Fig. 5. Figure 18 demonstrates that stator clocking in low aspect ratio geometries has different effects on performance at different span regions. Local effects on the loss coefficient are as much as ±0.025. The loss coefficients of the entire stator for all four

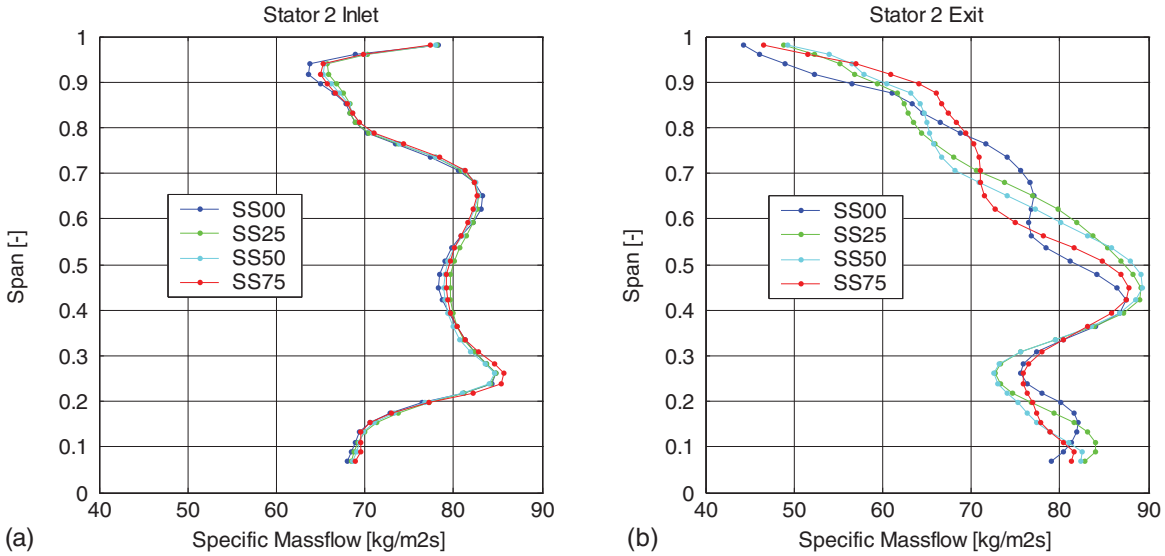

Fig. 16 Spanwise distribution of pitchwise mass-averaged area-specific massflow at stator 2: (a) inlet, (b) outlet

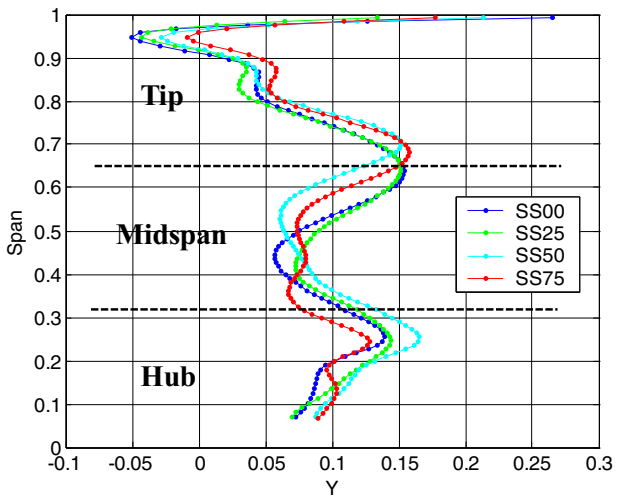

Fig. 17 Spanwise distribution of second stator total pressure loss coefficient Y of four stator-clocking positions

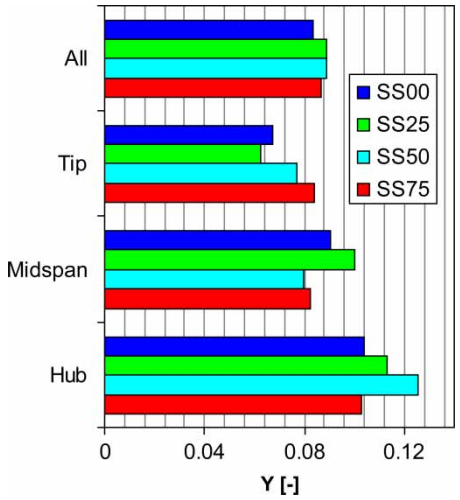

Fig. 18 Second stator total pressure loss coefficient Y of flow regions for different stator-clocking positions

clocking positions show only negligible differences of ±0.003. This observation confirms the findings of Behr *et al.* [**6**] that stator-clocking effects on performance in low aspect ratio geometries are likely to compensate each other.

It has been found that the 25 per cent clocking position (SS25) shows the lowest total pressure loss in the tip region, followed by the 0 per cent clocking position (SS00). At these two positions the secondary flow interaction region A passes the stator leading edge at its suction side (see Fig. 9). At the same positions the total pressure loss across the second stator is largest in the midspan region. This observation reflects the fact that the high turbulent interaction region A convects more into the midspan region within the second stator. Accordingly the losses are reduced at the tip and increased at midspan of the stator. The opposite effect is visible for the other two clocking position of 50 and 75 per cent. At these positions the interaction region A either hits the leading edge of the stator or passes close to the pressure side. In these cases the total pressure loss is highest at the stator tip passage region and lowest at midspan.

The total pressure loss variation with clocking at midspan does clearly not correspond with the wake model, which describes the effect of clocking on performance. The region labelled 'midspan' does not show the lowest total pressure loss for the case that the

upstream stator wake impinges on the second stator leading edge. This is due to highly three-dimensional flow, which is also present in the midspan region.

The region summarized with 'hub' in Fig. 17 is characterized by complex flow interaction of the rotor hub passage vortex and a corner vortex. Both vortices are periodically strengthened by the influence of the first stator passage vortex. The interaction of both vortices affects the entire flow path region from the hub until 30 per cent span and yields a diffused flow field with a generally increased level of turbulence.

4 CONCLUSIONS

This experimental investigation studies the effects of stator clocking in high-pressure turbine stages on performance and on the unsteady interaction of stator and rotor secondary flows. The exit flow fields of the rotor and the second stator are measured with high temporal and spatial resolution using time-resolved and pneumatic pressure probe techniques. Thus, the investigation is based on detailed information about pressure, flow angle, turbulence intensity and temperature.

The exit flow field of the first stage of the high-pressure turbine is characterized by highly three-dimensional flow. About 60 per cent of the span is dominated by vortical structures. Thus, pure wake structures are of relatively little importance in the overall flow field. The conventional wake model is, therefore, found to be inappropriate to describe the effect of stator clocking on performance in high-pressure turbine stages.

It is seen that stator secondary flow features interact periodically with the secondary flows of the downstream rotor. The interaction regions are dominated by vortical structures, which are transported by the rotor to fixed positions at the inlet of the subsequent stator. These regions are identified in the time-averaged stationary frame of reference by reduced levels of total pressure and increased levels of turbulence intensity and entropy.

The time-averaged total pressure distribution at the exit of an embedded stator with low aspect ratio geometry has regions of total pressure deficit that are caused by the upstream rotor secondary flow, which cover up to 50 per cent of the stator flow path area. These low total pressure regions move periodically through the stator exit flow field with the frequency of the rotor blade-passing. They are characterized in addition by increased levels of turbulence intensity.

The spanwise distributions of total pressure loss and massflow within the second stator are defined by the circumferential position of the vortex interaction regions at the inlet of the stator. This investigation shows that stator clocking in high-pressure turbine stages has a non-uniform effect on the performance of a downstream stator across the span, due to the highly three-dimensional flow. The integral change of performance due to clocking is marginal.

These findings indicate that multi-row interaction effects of vortical secondary flow features dominate the loss creation in low aspect ratio turbine geometries. With stator clocking these interactions can be modified in order to control the distribution of loss in downstream blade rows. The design process of high-pressure turbines should include unsteady multi-row CFD to account for vortex interaction and transport effects.

REFERENCES

1 **Huber, F. W., Johnson, P. D., Sharma, O. P., Staubach, J. B.,** and **Gaddis, S. W.** Performance improvement through indexing of turbine airfoiles: part 1 – experimental investigation. *ASME, J. Turbomach.*, 1996, **118**, 630–635.

2 **Gombert, R.** and **Höhn, W.** Unsteady aero-dynamical blade row interactions in a new multistage research turbine – part 1: experimental investigation. ASME paper 2001-GT-0306, 2001.

3 **Reinmöller, U., Stephan, B., Schmidt, S.,** and **Niehuis, R.** Clocking effects in a 1.5 stage axial turbine – steady and unsteady experimental investigations supported by numerical simulations. *ASME, J. Turbomach.*, 2002, **124**, 52–60.

4 **Tiedemann, M.** and **Kost, F.** Some aspects of wake–wake interactions regarding turbine stator clocking. *ASME, J. Turbomach.*, 2001, **123**, 526–533.

5 **Bohn, D., Ren, J.,** and **Sell, M.** Influence of stator clocking on the unsteady three-dimensional flow in a two-stage turbine. *ASME, J. Turbomach.*, 2005, **127**, 156–163.

6 **Behr, T., Porreca, L., Mokulys, T., Kalfas, A. I.,** and **Abhari, R. S.** Multistage aspects and unsteady flow effects of stator and rotor clocking in an axial turbine with low aspect ratio blading. *ASME, J. Turbomach.*, 2006, **128**, 11–22.

7 **Schennach, O., Woisetschläger, J., Fuchs, A., Göttlich, E, Marn, A.,** and **Pecnik, R.** Experimental invstigations of clocking in a one and a half stage transonic turbine using laser-doppler-velocimetry and a fast response aerodynamic pressure probe. ASME paper GT2006-90264, 2006.

8 **Arnone, A., Marconcini, M., Scotti del Greco, A.,** and **Spano, E.** Numerical investigation of three-dimensional clocking effects in a low pressure turbine. *ASME, J. Turbomach.*, 2004, **126**, 375–384.

9 **Haldeman, C. W., Dunn, M. G., Barter, J. W., Green, B. R.,** and **Bergholz, R. F.** Experimental investigation of vane clocking in a one and one-half stage high pressure turbine. *ASME, J. Turbomach.*, 2005, **127**(3), 512–521.

10 **Gadea, J., Dénos, R., Paniagua, G., Billard, C. H.,** and **Sieverding, C. H.** Effect of clocking on the second stator pressure field of a one and a half stage transsonic turbine. ASME paper GT2004-53463.

11 **Hummel, F.** Wake–wake interaction and its potential for clocking in a transsonic high-pressure turbine. *ASME, J. Turbomach.*, 2002, **124**(1), 69–76.

12 **Miller, R. J., Moss, R. W., Ainsworth, R. W.,** and **Horwood, C. K.** Time-resolved vane-rotor interaction in a high-pressure turbine stage. *ASME, J. Turbomach.*, 2003, **125**(1), 1–13.

13 **Gaetani, P., Persico, G., Dossena, V.,** and **Osnaghi, C.** Investigation of the flow field in a HP turbine stage for two stator rotor axial gaps – part II: unsteady flow field. ASME paper GT2006-90556.

14 **Chaluvadi, V. S. P., Kalfas, A. I.,** and **Hodson, H. P.** Vortex transport and blade interactions in high pressure turbines. *ASME, J. Turbomach.*, 2003, **126**(3), 395–405.

15 **Behr, T., Kalfas, A. I.,** and **Abhari, R. S.** Unsteady flow physics and performance of a one-and-1/2-stage unshrouded high work turbine. *ASME, J. Turbomach.*, 2007, **129**(2), 348–359.

16 **Sell, M., Schlienger, J., Pfau, A., Treiber, M.,** and **Abhari, R. S.** The 2-stage axial turbine test facility LISA. ASME paper 2001-GT-0492, 2001.

17 **Behr, T., Kalfas, A. I.,** and **Abhari, R. S.** A probabilistic uncertainty evaluation method for turbomachinery probe measurement. In Proceedings of the XVIIIth Bi-Annual Symposium on Measuring Techniques in Transonic and Supersonic Flows in Cascades and Turbomachines, Thessaloniki, Greece, 21–22 September 2006.

18 **Kupferschmied, P., Köppel, O., Gizzi, W. P.,** and **Gyarmathy, G.** Time resolved flow measurements with fast aerodynamic probes in turbomachinery. *Meas. Sci. Technol.*, 2000, **11**, 1036–1054.

19 **Pfau, A., Schlienger, J., Kalfas, A. I.,** and **Abhari, R. S.** Virtual four sensor fast response aerodynamic probe (FRAP). In Proceedings of the XVIth Bi-Annual Symposium on Measuring Techniques in Transonic and Supersonic Flows in Cascades and Turbomachines, Cambridge, UK, 23–24 September 2002.

20 **Porreca, L., Hollenstein, M., Kalfas, A. I.,** and **Abhari, R. S.** Turbulence measurements and analysis in a multistage axial turbine. ISABE Conference Paper 2005-1032, Munich, Germany, 2005.

21 **Denton, J. D.** Loss mechanisms in turbomachines. *ASME, J. Turbomach.*, 1993, **115**(4), 621–656.

22 **Chaluvadi, V. S. P., Kalfas, A. I.,** and **Hodson, H. P.** Blade row interaction in a high pressure turbine. *J. Propuls. Power*, 2001, **17**(4), 892–901.

23 **Dejc, M. E.** and **Trojanovskij, B. M.** *Untersuchung und Berechnung Axialer Turbinenstufen*, 1973 (VEB Verlag Technik, Berlin).